Naval Research Laboratory

Washington, DC 20375-5320

NRL/MR/6394--19-9785

Modeling Powder-Based Additive Manufacturing Processes for Functional Tailoring

John C. Steuben
Athanasios P. Iliopoulos
Andrew J. Birnbaum
John G. Michopoulos

Center for Materials Physics and Technology
Materials Science and Technology Division

March 11, 2019

REPORT DOCUMENTATION PAGE

Form Approved
OMB No. 0704-0188

1. REPORT DATE *(DD-MM-YYYY)*
11-03-2019

2. REPORT TYPE
Memorandum Report

3. DATES COVERED *(From - To)*
17JAN2017 - 16JAN2018

4. TITLE AND SUBTITLE

Modeling Powder-Based Additive Manufacturing Processes for Functional Tailoring

(Modeling AM for Functional Tailoring)

5a. CONTRACT NUMBER
core

5b. GRANT NUMBER
core

5c. PROGRAM ELEMENT NUMBER
61153N

6. AUTHOR(S)

John C. Steuben, Athanasios P. Iliopoulos, Andrew J. Birnbaum and John G. Michopoulos

5d. PROJECT NUMBER

5e. TASK NUMBER

5f. WORK UNIT NUMBER
N2L5

7. PERFORMING ORGANIZATION NAME(S) AND ADDRESS(ES)

Naval Research Laboratory
4555 Overlook Avenue, SW
Washington, DC 20375-5320

8. PERFORMING ORGANIZATION REPORT NUMBER

NRL/MR/6394--19-9785

9. SPONSORING / MONITORING AGENCY NAME(S) AND ADDRESS(ES)

Office of Naval Research
875 N. Randolph Street
Arlington, VA 22203

10. SPONSOR / MONITOR'S ACRONYM(S)

ONR

11. SPONSOR / MONITOR'S REPORT NUMBER(S)

12. DISTRIBUTION / AVAILABILITY STATEMENT

DISTRIBUTION STATEMENT A: Approved for public release; distribution is unlimited.

13. SUPPLEMENTARY NOTES

14. ABSTRACT

The purpose of this document is to describe research primarily conducted by John C. Steuben under a Karle's Fellowship.

15. SUBJECT TERMS
Additive Manufacturing; Functional Tailoring; Process Control; Discrete Element Methods; Analytic Solutions; Topology Optimization; Multi-scale Optimization

16. SECURITY CLASSIFICATION OF:			17. LIMITATION OF ABSTRACT	18. NUMBER OF PAGES	19a. NAME OF RESPONSIBLE PERSON
					John C. Steuben
a. REPORT	**b. ABSTRACT**	**c. THIS PAGE**			**19b. TELEPHONE NUMBER** *(include area code)*
Unclassified Unlimited	Unclassified Unlimited	Unclassified Unlimited	Unclassified Unlimited	20	(202) 404-1532

Standard Form 298 (Rev. 8-98)
Prescribed by ANSI Std. Z39.18

This page intentionally left blank.

CONTENTS

FIGURES

This page intentionally left blank.

EXECUTIVE SUMMARY

To determine the operational parameters that control powder based Additive Manufacturing (AM) processes, in order to manufacture functionally tailored Navy-relevant parts, the development of proper process theories and models is necessary. The specific objective of the work described in this document was the development of the analytical and computational infrastructure for modeling and simulating the as-produced geometric and functional properties of objects produced via powder-based AM processes.

This page intentionally left blank.

MODELING POWDER-BASED ADDITIVE MANUFACTURING PROCESSES FOR FUNCTIONAL TAILORING

1. RESEARCH SUMMARY

The research effort associated with this Karles Fellowship program was devoted to modeling and simulation efforts applicable to the domain of Additive Manufacturing (AM). One major research accomplishment was the development of the Multiphysics Discrete Element Method (MDEM) and implementation of the NRL Additive Manufacturing Multiphysics Discrete Element Method (NAMMDEM). This effort is described in Section 1. Another major goal of this project was the development of Enriched Analytic Solution Methods (EASMs), in order to model the thermo-mechanical aspects of AM processes in a highly computationally efficient manner, as part of an effort to achieve real-time process feedback control. This work is described in Section 2. This work also resulted in the development of new multi-scale topology optimization techniques which utilize the unique meso-scale structuring capability provided by AM in order to functionally tailor components in order to optimize performance. This spin-off effort is described in Section 3. Collectively, these accomplishments represent substantial progress towards the goal of enabling AM for performance-critical, Navy-relevant applications. They have resulted in great interest from Navy partners in academia and industry, as well as numerous publications, conference publications, and patent applications.

2. MULTIPHYSICS DISCRETE ELEMENT METHOD

Powder-based AM is based on the concept of fusing fine granules of material using the directed application of energy (e.g. a laser or electron beam). The focus of this project was the development of a Multiphysics Discrete Element Method (MDEM) suitable for modeling and simulation of such processes. MDEM is a finite-difference numerical method for simulating the behavior of both continuous and discontinuous material systems, based on the Newtonian interactions of a system of particles. These particles are imbued with constitutive behaviors including contact/collision models, heat transfer models, the ability to form and break inter-particle bonds, and respond to external fields.

An MDEM simulation contains a number of particles, a subset of which may be "bonded," or attached to each other. To the extent that they contact each other both bonded and unbonded particles participate in Newtonian collisions that produce reaction forces. These forces in turn propagate into changes in particle velocity and position. A schematic overview of the associated concepts from the perspective of interacting particles is shown in Fig. 1.

2.1 Methodology

Particle collision detection is performed using a dynamically-optimized octree augmented by Verlet lists. A inter-particle contact formulation incorporating thermoplasticity is employed. Bonds are formed based on a thermal criterion, and are also modeled as 1D linear elastic elements, and are assumed to fail instantaneously when a critical stress level is reached. Both particle contacts and bonds mediate the conduction

Manuscript approved January 9, 2019.

[b]

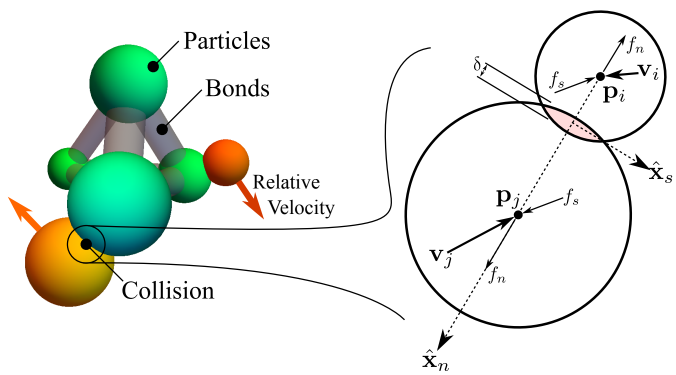

Fig. 1: Overview of the MDEM. At right, the variables associated with the collision mechanics are diagrammed.

of heat; particle radii and bond length are modeled as a linear function of temperature in order to simulate thermal expansion/contraction. A two-dimensional visualization example of the bonding process is shown in Fig. 2.

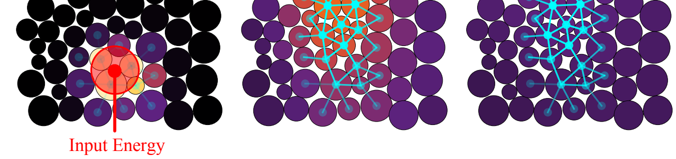

Fig. 2: Illustration of bond formation due to a concentrated heat source moving in the upwards direction. Particle hue corresponds to temperature. Bond opacity corresponds to a general notion of bond strength.

The particles in the MDEM simulation experience interactions with the build domain, namely those of gravity, viscous drag, the laser heat source, and collisions with stationary or moving planes. The planar boundary conditions are utilized to construct a “scraper” arrangement that closely mimics the physical AM process, which is diagrammed in Fig. 3. The laser heat source is modeled as a uniform circular heat source of constant radius, the position of which is dictated by a precomputed series of directives known as "G-code." Gas pressure "denudation" effects associated with the heat source are also modeled as shown in Fig. 4.

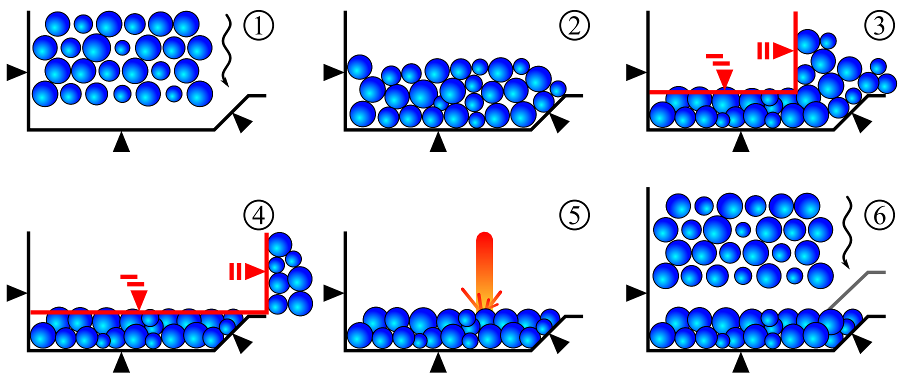

Fig. 3: Overview of the scraper boundary conditions for particle compaction. 1) Particles introduced 2) Settling. 3) Scraping and compaction. 4) Deletion of excess particles. 5) Laser power applied. 6) The process begins again.

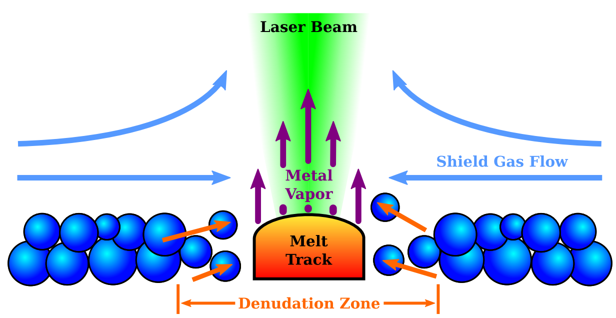

Fig. 4: Illustration of the denudation process. The incident laser beam causes an upward flux of metal vapor, drawing in shield gas and feedstock particles.

Time-step integration for the Newtonian mechanics of the MDEM is performed using the symplectic velocity-Verlet integrator, while the implicit Euler method is used to solve the heat equation. A novel selective physics deactivation technique is used to improve computational efficiency, as shown in 5. The NAMMDEM implementation of the MDEM formulation is a high-performance C++ code, and employs shared-memory parallelization via Open-MP. A custom graphics engine for visualizing huge numbers of particles was developed using OpenGL and the Qt cross-platform framework. A “metaball” technique is used to visualize the solidified result of the AM process, as shown in Fig. 6.

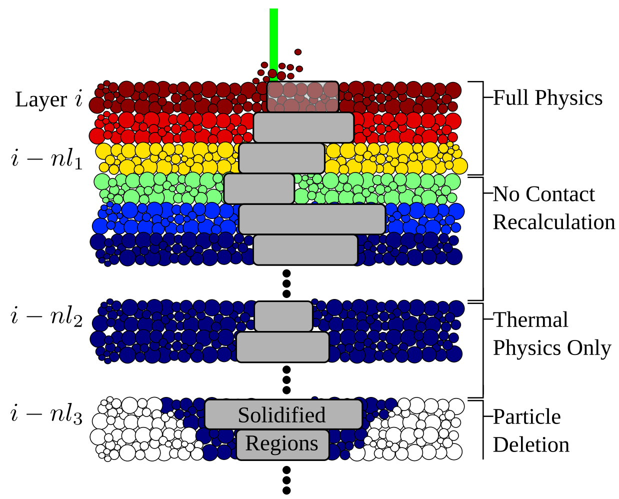

Fig. 5: Illustration of layer deactivation. The top layers experience all physics. Layers nl_1 to nl_2 omit the octree searching for new potential collisions. Layers nl_2 to nl_3 compute heat fluxes and temperatures only. Below layer nl_3, particles may be removed if they are unbonded and experience no heat flux.

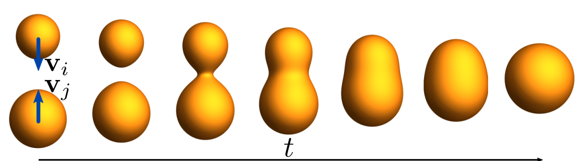

Fig. 6: Illustration of a metaball. Two particles of different radii move towards one another, snapshots of the metaball surface shown at various points in time, advancing from left to right.

2.2 Demonstration Results

In order to demonstrate the application of NAMMDEM tool to a large-scale test problem, the construction of a mechanical component was simulated. In this case, the geometry of a connecting rod cap was used. The corresponding geometry model input to the slicer is shown in Fig. 7. In the present work a quarter-symmetry model is simulated. The geometry was scaled to a height of 5mm, and a 0.1mm layer thickness was specified. Material properties corresponding to 316-L stainless steel were used. The metaball representation of the final geometry output is given in Fig. 8.

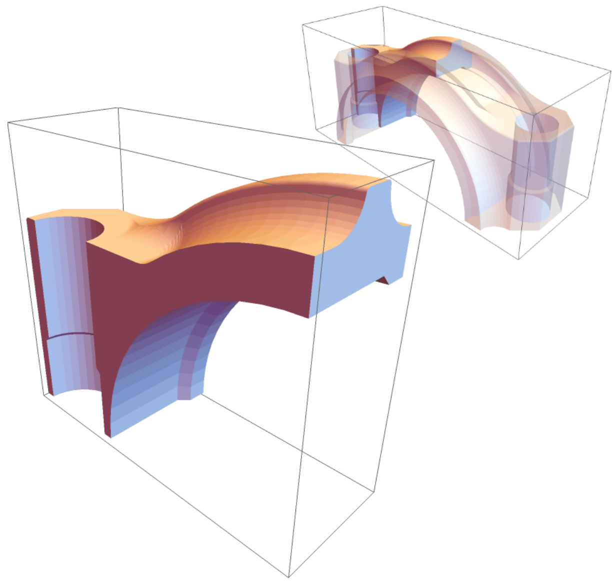

Fig. 7: Connecting rod quarter-symmetry model, with full model inset.

In the metaball display of Fig. 8 the layered nature of the AM build process is quite evident. The surface texture of the completed component is also clearly shown. Several gross defects from the printing process may be observed, the most notable of which is a major delamination between layers about half-way up the build volume. Figure 9 shows the cause of this defect: warping during the cooling of one layer results in the recoater blade strike on the next, which gouges material out of the build domain. To the best of our knowledge, no other simulation technique for AM has demonstrated the capability to capture these effects and the resultant features.

3. ENRICHED ANALYTIC SOLUTION METHODS

Despite the high computational performance of the NAMMDEM implementation, several hours or days are required to deliver simulation results. While this is highly useful for some activities, it is not adequate if the model is to be used “in the loop” to achieve real-time process feedback control. To be used in such a role, a model must be able to produce results in a small fraction of a second. Under such constraints, an appropriate modeling approach is to attempt the “enrichment” of classical analytical solutions to the heat equation in order to capture the relevant physics of AM.

3.1 Methodology

Classical solutions to the heat equation, such as those of Rosenthal or Eager & Tsai, are exact solutions over homogeneous semi-infinite domains only. While these solutions are directly applicable to problems such as laser welding, they are of limited utility in the domain of AM. Issues to be addressed include:

1. Non-convex, topologically complex finite domains present in AM,

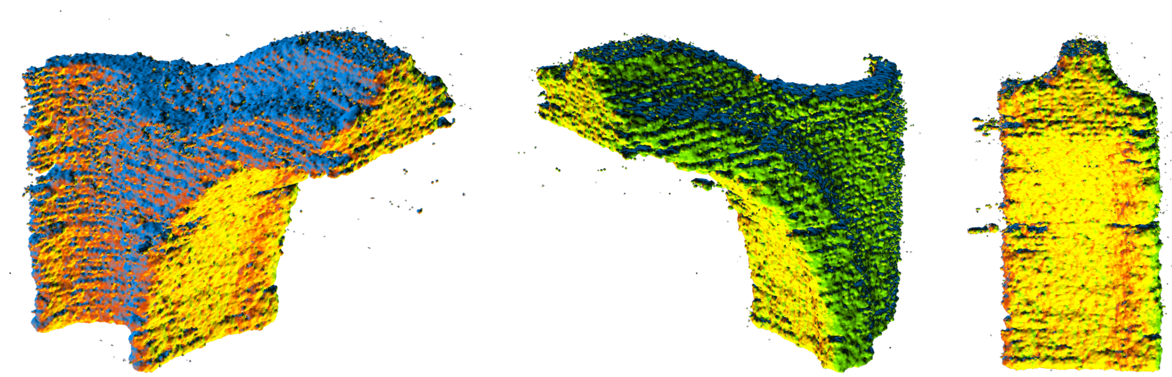

Fig. 8: Multiple views of the metaball representation of the MDEM output from the connecting rod cap problem. Coloration corresponds to surface normal direction, in order to show texture.

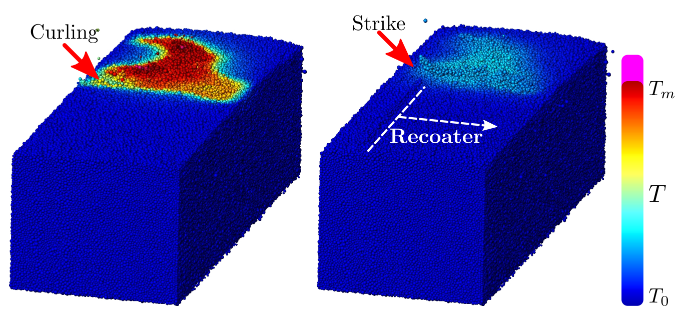

Fig. 9: Illustration of layer curling during cooling (left) and subsequent recoater blade strike (right) causing the expulsion of material.

2. Inhomogeneous material throughout the AM domains, and

3. Strong, nonlinear variation in material properties as a function of temperature.

In order to address the first of the two enumerated issues, we employed the so-called "method of images." The heat source associated with the AM process within the part domain is augmented by a *mirror* source outside the domain, in order to produce a temperature distribution symmetric about the domain boundary. Systematic corrections to the traditional method of images are required in cases where the heat source is very close to the edge of the domain. The third issue is addressed by an iterative scheme, where the analytic solution is repeatedly evaluated, with material properties recomputed for each subsequent evaluation. The mathematical details of the technique are numerous, and will be the subject of upcoming publications. The effectiveness of this technique is best demonstrated by direct comparison to conventional numerical methods such as Finite Element Analysis (FEA).

3.2 Demonstration Results

To provide a demonstration of the capabilities of the EASM method, and compare its results to an established FEA implementation, a simple test problem was devised. A Gaussian laser heat source scans along the boundary of a finite domain, around an interior (concave) corner of the part being manufactured as shown in Fig. 10. A mirror heat source is also computed and corrected for proximity effects. The domain is modeled with the temperature dependent properties of Ti6Al4V as shown in Figure 11.

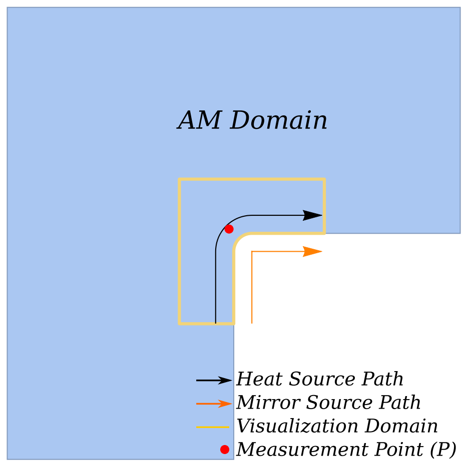

Fig. 10: Illustration of the EASM test problem domain.

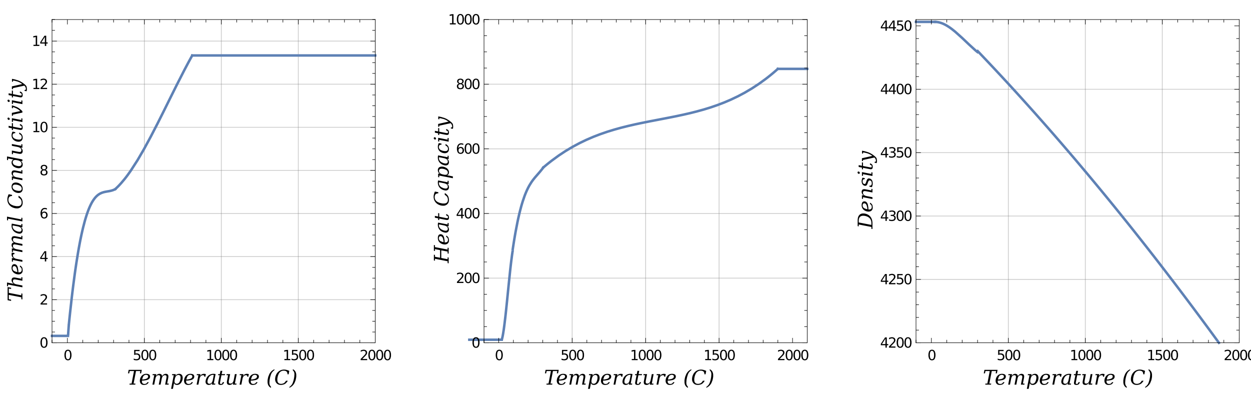

Fig. 11: Thermophysical properties of Ti6Al4V as a function of temperature.

Fig. 12 shows the temperature at point *P* as a function of time as the laser (and mirror) sources move along their prescribed paths. Fig. 13 shows the temperature distribution over the subdomain indicated in Fig. 10 at the moment the heat source reaches the end of its path. In both figures it is clear that the unenriched analytic model is clearly not capable of adequately capturing the thermal physics of the finite geometric domain. The uncorrected EASM using the method of images without corrections also exhibits poor accuracy. The final ouptput of this research, however, delivers a prediction which is nearly identical to that of the FEA model. This indicates that the EASM framework is capable of delivering results equivalent to those of the much more expensive FEA model. We note that the FEA simulation required approximately 20 minutes on a 12-core workstation computer. An un-optimized serial implementation of the EASM requires 100 *microseconds* to evaluate the temperature at a single point. The EASM framework therefore offers an increase of six orders of magnitude in relevant circumstances, and is sufficiently performant for “in the loop” use.

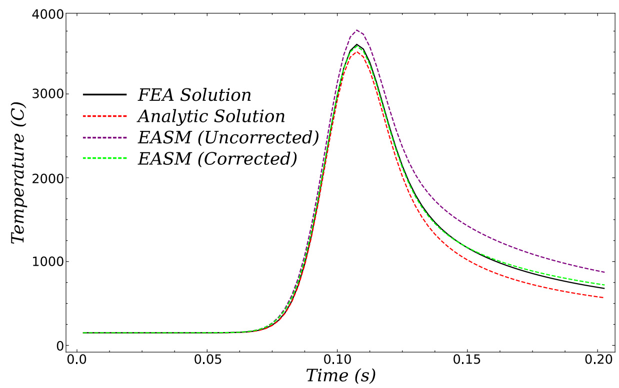

Fig. 12: Temperature history at point P for a reference FEA model (Black), un-enriched analytical model (Red, Dashed), EASM (Purple, Dashed) and corrected EASM (Gree, Dashed).

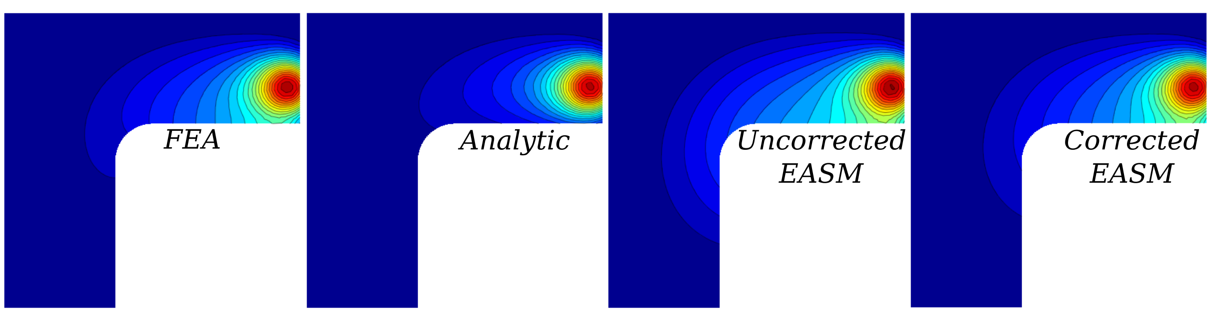

Fig. 13: Thermal field comparison between FEA, Analytic, and EASM models.

4. MULTISCALE TOPOLOGY OPTIMIZATION FOR AM

As a result of the research described previously, we realized that AM offered a unique capability for structuring the *mesoscale* of fabricated components in order to functionally tailor their properties for their intended use. This work constitutes a novel multiscale approach that is enabled by combining an implicit slicing methodology acting at the meso-scale with a traditional topology optimization for the macro-scale. This allows the optimization of both the macro and meso-structures in order to improve the mechanical performance of the resulting components. More broadly, this work presents modifications to the additive manufacturing digital thread that enable tailoring the response of additively manufactured structures with respect to performance specifications.

4.1 Methodology

To address the issue of tailoring the slicing in a manner that enables the part to respond optimally under its usage conditions, we developed a novel methodology known as "implicit slicing." The implicit slicer is based on computing the level sets of functional fields defined over the spatial domain of the object to be manufactured. This formulation elegantly solves the problem of computing polygon offsets for arbitrary (and possibly degenerate) geometries, but it allows the introduction of "design intent" into the digital thread. Since the field(s) upon which the infill toolpaths are computed may be specified by the user, this function may be chosen based on performance criteria. An example, illustrated in Fig. 14 shows the use of the von Mises stress in order to generate the infill for a dogbone test specimen. Experimentation showed that the meso-scale toolpath tailoring of the implicit slicer produced parts with mechanical performance superior to those exhibited by parts produced using conventional slicers.

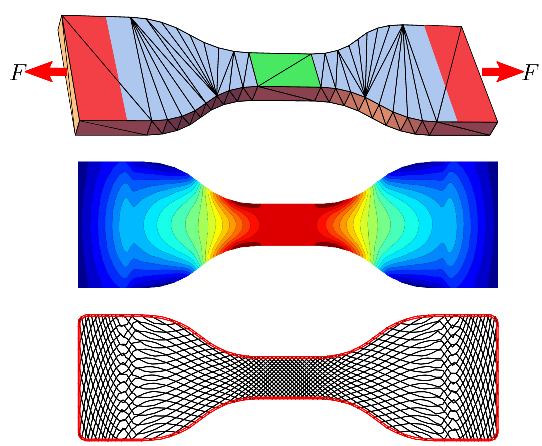

Fig. 14: Example of implicit slicing. At top, the input geometry and applied force F. At center, the von Mises stress in the part, as calculated using Finite Element Analysis. At bottom, the toolpath produced by the implicit slicer.

The term Topology Optimization (TO) refers to a diverse family of methods that seeks to optimize the distribution of material within a given design space, for a given set of boundary conditions, with the goal of maximizing a measure of performance of the resulting structure. Alternatively, topology optimization can be imagined as the process of determining where to "poke holes" in a structure or where to deposit material in a design volume, in order to reduce its mass, without compromising performance.

It is clear that there is a strong conceptual link between topology optimization and implicit slicing. The purpose of TO is to produce a density function that describes the optimal distribution of material within the original domain. The implicit slicer, on the other hand, accepts a function describing where material should be distributed (in order to achieve a functional performance goal) and produces an output toolpath for AM hardware based on this function. Previous applications of the implicit slicer have used common measures such as von Mises stress to indirectly capture the notion of where material should be concentrated in order to improve performance. The use of topology optimization notably improves this situation, since its output is a direct measurement of where material should be placed. It is clear that the two tools can be easily linked by first conducting the topology optimization, and subsequently invoking the implicit slicer. In practice, there are numerous details associated with the coupling of these two methodologies in a manner that enables multiscale tailoring of mass deposition topology associated with AM processes. An schematic overview of the proposed is depicted schematically by the workflow in Fig. 15.

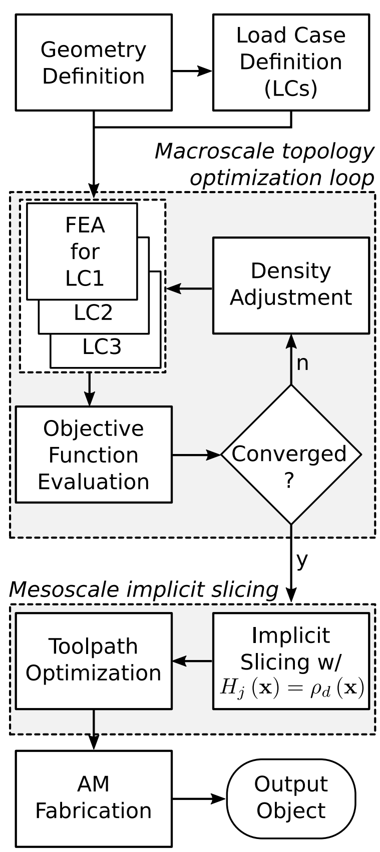

Fig. 15: Flowchart of the workflow demonstrating the stages of the proposed multiscale methodology for topology optimization.

4.2 Demonstration Results

The approach outlined in the previous section allows the practical application of multiscale topology optimization for common engineering design problems. We sought to find an illustrative example of this capability, and found such an example during the construction of a uniaxial test machine. We required a spanner wrench to adjust the oddly-shaped fasteners pictured in Fig. 16. The wrench for such a nut must be compact, lightweight, and support the load applied to tighten the fastener; an ideal candidate for topology optimization. The initial domain for the wrench geometry, along with applied loads and constraints, are also shown in Fig. 16.

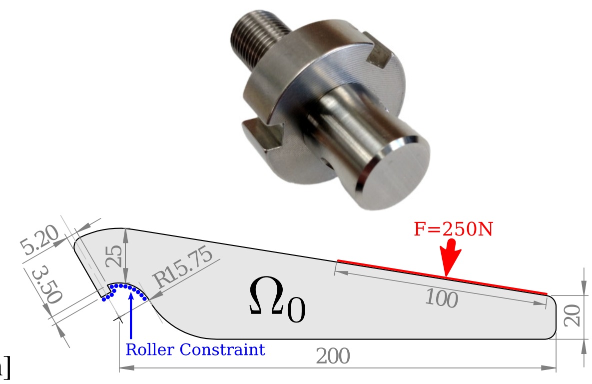

[h]

Fig. 16: The fastener that the spanner must drive (top), and the corresponding dimensions and boundary conditions on the outer envelope of the spanner wrench.

The methodology outlined previously was applied, The implicit slicing required approximately 1 second per layer (50s total) of computation time on a dual-core laptop computer. The topology optimizer and implicit slicer results, along with the final toolpath may be seen in Fig. 17. The output toolpath was formatted into “g-code” for a FDM 3D printer. Printing of the wrench required approximately 20 minutes. The finished component may be seen in Fig. 17f. We note that the wrench is of adequate strength for the task of tightening the fastener shown.

On one hand the present work offers an immediate path forward for the production of lightweight functional structures using AM. On the other hand, viewed more broadly, the present work represents one possible path towards an improved digital thread such as that shown in Fig. 18. We imagine that the various steps in the existing digital thread, which are largely based on heuristics, may be replaced by an “design optimization environment” that encapsulates the present work. Importantly, the steps in the optimization environment are driven by algorithms that explicitly seek to tailor the AM component for some functional purpose. Additionally, the geometric input of the digital thread is replaced with a design specification, which includes geometry and functional specifications such as boundary conditions. The production environment remains unchanged, reflecting the desire to make the reinterpreted digital thread compatible with existing hardware systems.

Although the present work represents only the initial steps towards one possible reimagining the digital thread, it shows great potential. Despite the magnitude of future research effort that remains, the idea of multiscale topology optimization via combining TO with implicit slicing to achieve multiscale TO has been shown to offer unique possibilities for realizing many benefits of additive manufacturing that are currently unavailable and can be further extended to apply beyond structural to multiphysics performance requirements.

[!h]

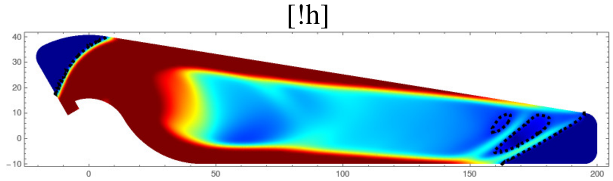

(a) $\rho_d(\mathbf{x})$.

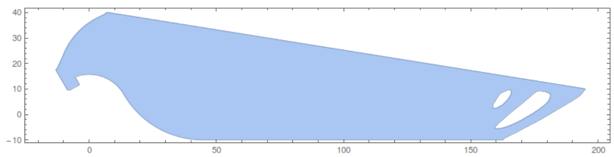

(b) Ω.

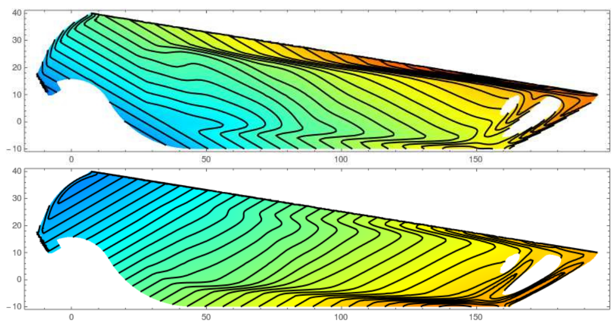

(c) H_{in} for $z = 0$ and $z = l_t$.

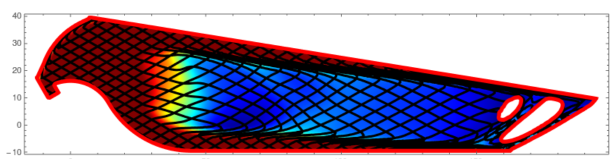

(d) $\rho_d(\mathbf{x})$ with $g_{in} \cup g_{pr}$ superimposed.

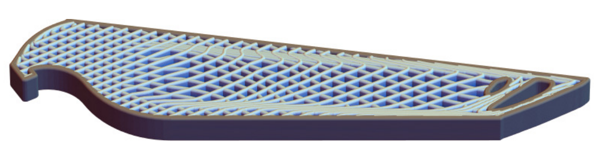

(e) Output toolpath.

(f) Photograph of as-manufactured wrench.

Fig. 17: Multiscale topology optimization of the wrench. At top (a) is the density function computed by the topology optimizer. Below (b) is the domain Ω upon which the implicit slicer operates. The infill function H_{in} is shown, for the first two layers, in (c). In (d) and (e) the output toolpath can be seen. At bottom (f) the FDM-manufactured wrench is photographed.

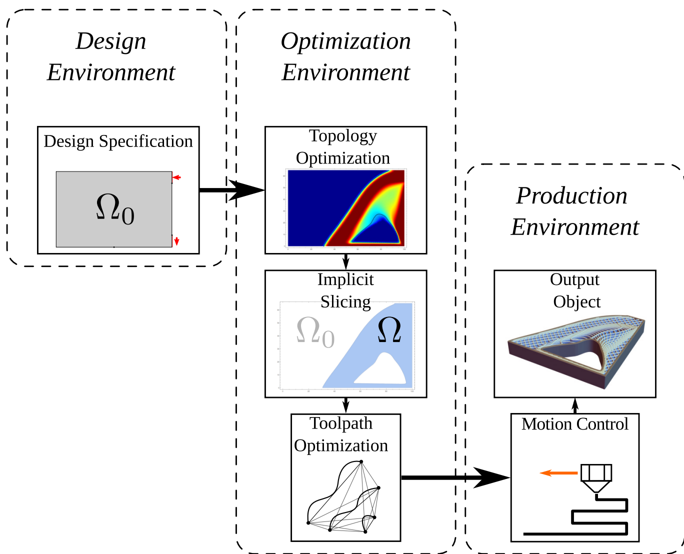

Fig. 18: The reinterpreted digital thread incorporating an optimization environment.